Proposing an Acquisition Geometry That Optimizes Super-Resolution in Digital Breast Tomosynthesis

Raymond J. Acciavatti and Andrew D.A. Maidment

University of Pennsylvania, Department of Radiology, Physics Section, 1 Silverstein Building, 3400 Spruce St., Philadelphia PA 19104-4206
racci@seas.upenn.edu, Andrew.Maidment@uphs.upenn.edu

Abstract. In digital breast tomosynthesis (DBT), oblique x-ray incidence shifts the image of an object in sub-pixel detector element increments with each projection angle. Our previous work has shown that DBT is capable of super-resolution as a result of this property. Although super-resolution is achievable over a broad range of positions for frequencies parallel to the chest wall side of the breast support, it is feasible at fewer positions for frequencies perpendicular to the chest wall. This finding arises because translational shifts in the image between projections are minimal in the chest wall-to-nipple direction. To optimize super-resolution, this work proposes an acquisition geometry in which the detector is translated in the chest wall-to-nipple direction between projections. At various increments of detector translation, we calculate the reconstruction of a sine input whose frequency is greater than the detector alias frequency. The model gives a proof-of-principle justification that detector translation promotes super-resolution.

Keywords: Digital breast tomosynthesis (DBT), aliasing, super-resolution, image reconstruction, Fourier Transform, spectral leakage, precision translation, optimization.

1 Introduction

In digital breast tomosynthesis (DBT), a 3D image of the breast is generated from a limited range of low-dose x-ray projections. Early clinical trials show that DBT has improved sensitivity and specificity for cancer detection relative to 2D digital mammography (DM), the current gold standard for breast cancer screening [1].

In DBT, the image of an object is translated in sub-pixel detector element increments with each increasing projection angle. Our previous work has demonstrated that DBT is capable of super-resolution (*i.e.*, sub-pixel resolution) as a result of this property [2]. The existence of super-resolution is dependent on the directionality of the input frequency and on position in the reconstruction. Although super-resolution is feasible over a broad range of positions for frequencies parallel to the chest wall side of the breast support, it is achievable at fewer positions for frequencies oriented along the posteroanterior (PA) direction. For example, super-resolution along the PA direction is not possible for input objects within the

A.D.A. Maidment, P.R. Bakic, and S. Gavenonis (Eds.): IWDM 2012, LNCS 7361, pp. 386–393, 2012.

mid-plane perpendicular to the chest wall and to the breast support. Since this mid-plane has extent in both the PA and source-to-support (SS) directions, it will be termed the mid PA/SS plane throughout the remainder of this work (Figure 1).

Super-resolution along the PA direction is not feasible in the mid PA/SS plane because translational shifts in the image between projections are minimal. To optimize super-resolution, this work proposes an acquisition geometry in which the detector is translated in the PA direction between projections. This design feature can be implemented through precision translation of the detector.

2 Methods

An analytical model of super-resolution is developed by calculating the reconstruction of a sine input whose frequency is greater than the alias frequency of the detector. Defining the xz plane as the chest wall (Figure 1), the input is taken to be a rectangular prism whose attenuation coefficient varies sinusoidally along the y direction. The input is positioned between the heights $z = z_0 \pm \varepsilon/2$ above the detector, where z_0 is the central height of the input and ε is its thickness (Figure 2). Denoting C as the amplitude of the waveform and f_0 as its frequency, the attenuation coefficient $\mu(x, y, z)$ can be written as $C \cdot \cos(2\pi f_0 y) \cdot \text{rect}[(z - z_0)/\varepsilon]$. The 1D Fourier transform of the input along the y direction is a sum of delta functions peaking at the frequencies $f_y = \pm f_0$. Since only the positive frequency is of interest in a physical measurement, this input is useful for modeling the reconstruction of a single input frequency.

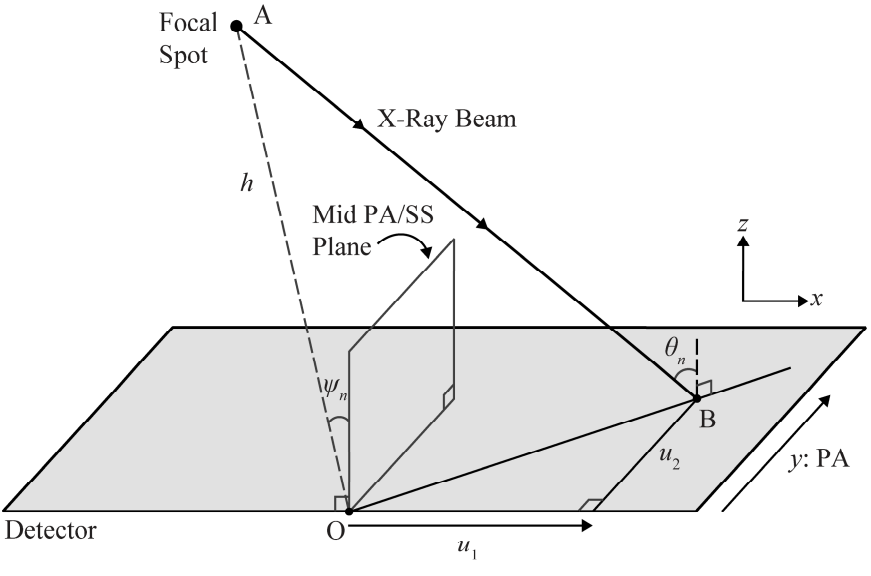

Fig. 1. In DBT, the n^{th} x-ray projection is acquired within the plane of the chest wall (*i.e.*, the xz plane) at the angle ψ_n relative to the z axis.

In DBT, x-ray projections are acquired as the x-ray tube rotates in a circular arc within the plane of the chest wall. In many systems, the midpoint of the chest wall side of the detector serves as the center-of-rotation (COR) of the x-ray tube. Defining the origin O as the COR, the vector from O to any point A in the tube's arc is thus $\overrightarrow{\mathrm{OA}} = (-h\sin\psi_n)\mathbf{i} + (h\cos\psi_n)\mathbf{k}$, where $\psi_n = n\cdot\Delta\psi$. In these expressions, h denotes the source-to-origin distance, ψ_n is the projection angle, n is the projection number, and $\Delta\psi$ is the angular spacing between projections. In a system with N total projections, the index n varies from $+(N-1)/2$ to $-(N-1)/2$ during the scan time.

The incident angle can now be calculated at any point B on the detector. Since $\overrightarrow{\mathrm{OB}} = u_1\mathbf{i} + u_2\mathbf{j}$, it follows that $\overrightarrow{\mathrm{BA}} = -\overrightarrow{\mathrm{OB}} + \overrightarrow{\mathrm{OA}} = -(u_1 + h\sin\psi_n)\mathbf{i} - u_2\mathbf{j} + (h\cos\psi_n)\mathbf{k}$, and hence the incident angle can be evaluated from the dot product

$$\cos\theta_n = \frac{\overrightarrow{\mathrm{BA}}\bullet\mathbf{k}}{\left|\overrightarrow{\mathrm{BA}}\right|\left|\mathbf{k}\right|}\ ,\ \theta_n = \arccos\left[\frac{h\cos\psi_n}{\sqrt{(u_1 + h\sin\psi_n)^2 + u_2^2 + (h\cos\psi_n)^2}}\right]. \tag{1}$$

Detector signal for each projection can now be determined by tracing the ray between points A and B. Defining w to be a free parameter, the equation of the ray can be written in terms of three parametric equations: $x = w(u_1 + h\sin\psi_n) - h\sin\psi_n$, $y = wu_2$, and $z = (1-w)h\cos\psi_n$. The focal spot at point A has been defined to correspond with $w = 0$, and the incident point at B has been defined to correspond with $w = 1$. The x-ray path length $\mathcal{L}_n$ through the input for the n^{th} projection is determined from the intersection of the incident ray with the planes $z = z_0 \pm \varepsilon/2$. The values of w for these two points are $w_n^{\pm} = 1 - (z_0 \pm \varepsilon/2)h^{-1}\sec\psi_n$. For the n^{th} projection, the total attenuation $\mathcal{A}\mu(n)$ is given by the integral $\int\mu ds$, where ds is the differential arc length along $\mathcal{L}_n$.

$$ds = \sqrt{\left(\frac{dx}{dw}\right)^2 + \left(\frac{dy}{dw}\right)^2 + \left(\frac{dz}{dw}\right)^2}\,dw = \sqrt{(u_1 + h\sin\psi_n)^2 + u_2^2 + (h\cos\psi_n)^2}\,dw \tag{2}$$

Combining Eqs. (1) and (2), it follows that $ds = h\cos(\psi_n)\sec(\theta_n)dw$. The total x-ray attenuation at the detector position (u_1, u_2) is thus

$$\mathcal{A}\mu(n) = \kappa_n\int_{w_n^+}^{w_n^-}\cos(2\pi f_0 u_2 w)dw = \frac{\kappa_n\left[\sin(2\pi f_0 u_2 w_n^-) - \sin(2\pi f_0 u_2 w_n^+)\right]}{2\pi f_0 u_2}\ , \tag{3}$$

where $\kappa_n = C\cdot h\cos(\psi_n)\sec(\theta_n)$. To simplify Eq. (3), recall the sum-to-product trigonometric identity $\sin(b_1) - \sin(b_2) = 2\cos[(b_1 + b_2)/2]\sin[(b_1 - b_2)/2]$ for real numbers b_1 and b_2.

$$\mathcal{A}\mu(n) = \kappa_n(w_n^- - w_n^+)\cos\left(\pi f_0 u_2\left[w_n^+ + w_n^-\right]\right)\mathrm{sinc}\left(f_0 u_2\left[w_n^- - w_n^+\right]\right) \tag{4}$$

$$= \frac{\varepsilon\kappa_n\sec\psi_n}{h}\cos\left(2\pi f_0 u_2\left[1 - \frac{z_0\sec\psi_n}{h}\right]\right)\mathrm{sinc}\left(\frac{\varepsilon f_0 u_2\sec\psi_n}{h}\right) \tag{5}$$

In Eq. (5), it is assumed that $\mathrm{sinc}(u) \equiv \sin(\pi u)/(\pi u)$. This expression for total attenuation implicitly assumes that the detector possesses an x-ray converter with a modulation transfer function (MTF) of unity at all frequencies. An amorphous selenium (*a*-Se) photoconductor operated in drift mode is a good approximation for an x-ray converter with this property [3].

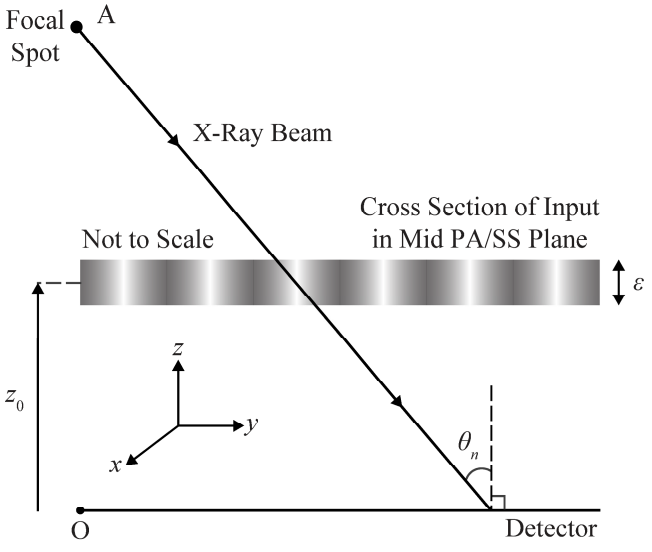

Fig. 2. In acquiring the central projection, a cross section of the input object in the mid PA/SS plane is shown. The attenuation coefficient varies sinusoidally along the PA direction (*y*).

In order to calculate the digitized detector signal, one must take into account the presence of a thin-film transistor (TFT) array which samples the total attenuation in pixels (*i.e.*, detector elements). The logarithmically-transformed signal for the n^{th} projection is found by averaging the signal over the $\mathbf{m}^{\text{th}}$ detector element

$$\mathcal{D}\mu(\mathbf{m},n) = \int_{a\left(m_y-\delta[n-(N-1)/2]\right)}^{a\left(m_y+1-\delta[n-(N-1)/2]\right)} \int_{a(m_x-1/2)}^{a(m_x+1/2)} \frac{\mathcal{A}\mu(n)}{a^2} \cdot du_1 du_2 \ , \ m_x \in \mathbb{Z} \ , \ m_y \in \mathbb{Z}^* \ . \qquad (6)$$

Detector elements are taken to be square with sides of length *a*. During the acquisition of the first projection for which $n = +(N-1)/2$, detector elements are centered on the coordinates $u_1 = m_x a$ and $u_2 = (m_y + 1/2)a$. In each subsequent projection, detector elements are translated in the PA direction (+*y*) by the amount δa, where δ is a parameter which expresses the translation between projections as a fraction of detector element length. Because θ_n should not vary considerably within each detector element, total attenuation can be approximated as

$$\tilde{\mathcal{A}}\mu(n) = \mathcal{A}\mu(n)\big|_{\theta_n=\theta_{\mathbf{m}n}} \ , \ \theta_{\mathbf{m}n} \equiv \theta_n\big|_{(u_1,u_2)=\left(m_x a, a\left[m_y+\frac{1}{2}-\delta\left(n-\frac{N-1}{2}\right)\right]\right)} \ , \qquad (7)$$

where $\theta_{\mathbf{m}n}$ is the evaluation of the incident angle at the centroid of each detector element. Hence

$$\mathcal{D}\mu(\mathbf{m},n) \cong \int_{a\left(m_y-\delta[n-(N-1)/2]\right)}^{a\left(m_y+1-\delta[n-(N-1)/2]\right)} \frac{\tilde{\mathcal{A}}\mu(n)}{a}\cdot du_2 = \lim_{J_y\to\infty}\frac{1}{J_y}\sum_{j_y=1}^{J_y}\tilde{\mathcal{A}}\mu(j_y,n)\ , \tag{8}$$

where

$$\tilde{\mathcal{A}}\mu(j_y,n) \equiv \tilde{\mathcal{A}}\mu(n)\Big|_{u_2=a\left(\frac{j_y-1/2}{J_y}+m_y-\delta\left[n-\frac{N-1}{2}\right]\right)}\ . \tag{9}$$

In Eq. (8), the midpoint formula has been used to evaluate the integral [4]. For the n^{th} projection, the signal $\mathcal{S}\mu(u_1, u_2)$ recorded by the detector can now be written as

$$\mathcal{S}\mu(u_1,u_2) = \sum_{\mathbf{m}}\mathcal{D}\mu(\mathbf{m},n)\,\text{rect}\left(\frac{u_1-m_x a}{a}\right)\text{rect}\left(\frac{u_2-a\left(m_y+\frac{1}{2}-\delta\left[n-\frac{N-1}{2}\right]\right)}{a}\right). \tag{10}$$

Using this expression, simple backprojection (SBP) reconstruction can be performed.

3 Results

Reconstructions are simulated for a DBT unit comparable to the Selenia Dimensions system (Hologic Inc., Bedford, MA) with 15 projections taken at an angular spacing ($\Delta\psi$) of 1.07°, assuming z_0 = 50.0 mm, ε = 0.5 mm, h = 70.0 cm, $C = 1/\varepsilon$ = 2.0 mm^{-1}, and a = 0.14 mm. To illustrate the potential for super-resolution, an input frequency (f_0) of 5.0 lp/mm has been chosen, since this frequency is higher than the detector alias frequency $0.5a^{-1}$ (3.6 lp/mm).

In a conventional geometry in which the detector is not translated between projections ($\delta = 0$), Figure 3(a) shows SBP reconstruction versus position y measured perpendicular to the chest wall at the height $z = z_0$ = 50.0 mm within the mid PA/SS plane ($x = 0$). Super-resolution is not achievable since translational shifts in the image of the object are minimal between projections. SBP reconstruction resembles a single projection whose signal varies with position y in a step-like manner, with the width of each step matching the detector element length. The corresponding 1D Fourier transform of SBP reconstruction along the y direction has a major peak at 2.7 lp/mm as evidence of aliasing [Figure 3(b)]. Although Figure 3(a) is plotted over the region $y \in$ [29.4 mm, 30.6 mm], similar plots hold over a broad range of y values.

By translating the detector in the PA direction between projections, super-resolution in the mid PA/SS plane can be achieved. Figure 3(a) considers translations of 25% of detector element length between projections ($\delta = 0.25$). The major peak of the Fourier transform [Figure 3(c)] correctly occurs at the input frequency, 5.0 lp/mm.

Due to the PA detector translations, it would initially seem that the new geometry has the drawback of loss of x-ray coverage at the chest wall with each successive projection. However, it can be shown that the net translation of the detector during the scan time is minimal; in this example, the net translation is $(N-1)\delta a$ or 0.49 mm. For this reason, the loss of x-ray coverage at the chest wall is negligible.

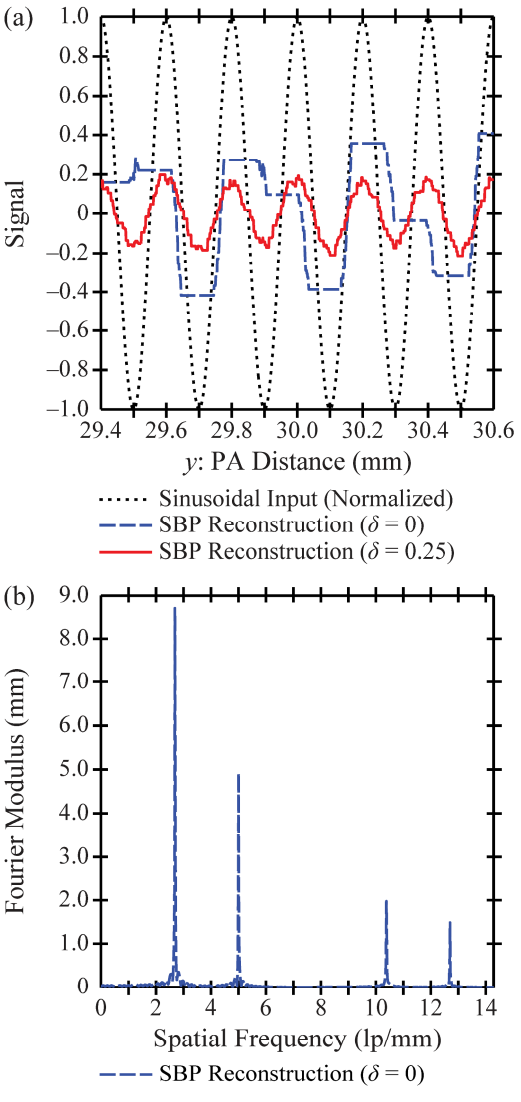

Fig. 3. Within the mid PA/SS plane, SBP reconstructions are plotted versus position y measured perpendicular to the chest wall for PA detector motions of 0% and 25% of detector element length between projections. The corresponding one-dimensional Fourier transforms along the y direction are also shown. The quality of super-resolution can be determined from the ratio (r) of the Fourier amplitudes at the aliased frequency (2.7 lp/mm) to the input frequency (5.0 lp/mm). By plotting this ratio versus δ, it is shown that super-resolution is not achievable at integer values of δ. That is, in order to maximize sub-pixel sampling gain between projections, the PA detector translation should occur in fractional multiples of detector element length.

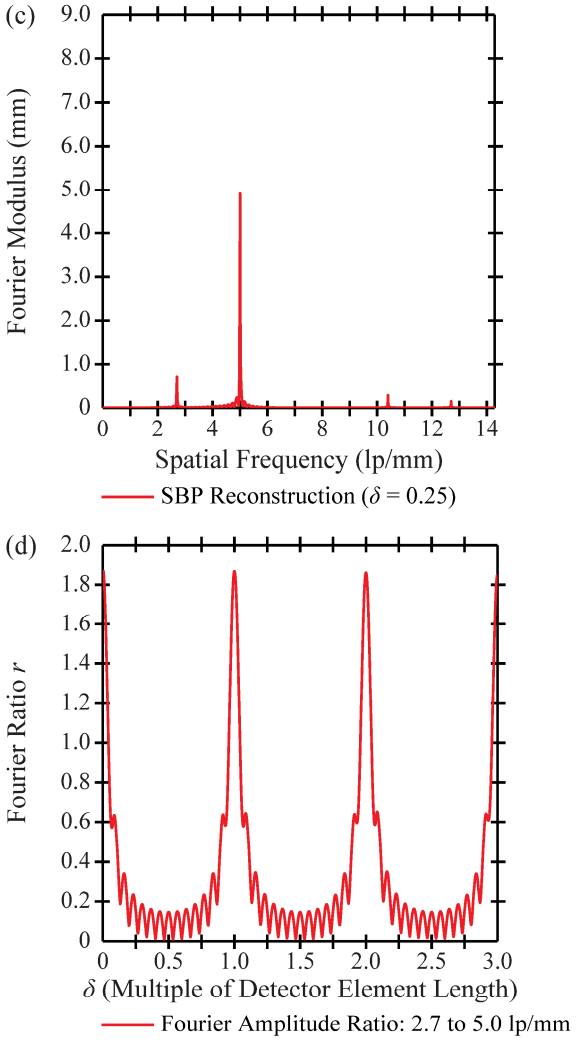

Fig. 3. (*continued*)

In order to assess the quality of super-resolution in the reconstruction, the ratio (r) of the amplitude of the Fourier peaks at 2.7 lp/mm to 5.0 lp/mm can be calculated. Super-resolution is present provided $r < 1$, and is absent provided $r \geq 1$. The dependency of r on δ is investigated in Figure 3(d). For measurements taken within the mid PA/SS plane, this plot illustrates that super-resolution along the PA direction is not feasible ($r > 1$) if detector translation between projections occurs in integer multiples of detector element length. To maximize sub-pixel sampling gain between projections, the PA translational shifts of the detector should occur in fractional multiples of detector element length. As shown in Figure 3(d), there is a relatively broad range of δ values over which r is sufficiently less than unity. For example, over

the range $\delta \in [0.24, 0.76]$, the ratio of the amplitude of the Fourier peaks at 2.7 lp/mm to 5.0 lp/mm is less than 1:5 (*i.e.*, 0.20). Consequently, the existence of super-resolution in the mid PA/SS plane is relatively insensitive to the precise translational shifts between projections, provided that these shifts are not sufficiently close to integer multiples of detector element length.

A DBT detector may be designed with either discrete or continuous translations in the PA direction during the scan time. Although this work implicitly considers discrete translations, continuous translations should also show super-resolution in the mid PA/SS plane, since the detector translation during a typical exposure time for each projection should be significantly smaller than the detector element length.

4 Discussion

We have shown that translating the detector in the PA direction between projections broadens the positions over which super-resolution is achievable in DBT. Although SBP reconstructions are useful for illustrating this concept as proof-of-principle, future work should be directed at incorporating filters into the reconstruction [5]. In addition, other subtleties of the imaging system, such as noise [6] and focal spot blurring [5], can be modeled.

There are additional acquisition geometries which promote super-resolution in DBT. Future studies will investigate whether super-resolution can be optimized with x-ray tube motion having a component in the y direction in addition to the x and z directions.

Acknowledgments. The project described was supported by predoctoral training grant No. W81XWH-11-1-0100 through the Department of Defense Breast Cancer Research Program. The content is solely the responsibility of the authors and does not necessarily represent the official views of the funding agency.

References

1. Rafferty, E.: Tomosynthesis: New Weapon in Breast Cancer Fight. Imaging Economics 17(4) (2004)
2. Acciavatti, R.J., Maidment, A.D.A.: Investigating the potential for super-resolution in digital breast tomosynthesis. In: Pelc, N.J., Samei, E., Nishikawa, R.M. (eds.) Proc. of SPIE, Medical Imaging 2011: Physics of Medical Imaging, vol. 7961, pp. 79615K-1–79615K-12. SPIE, Bellingham (2011)
3. Lee, D.L., Cheung, L.K., Rodricks, B., Powell, G.F.: Improved imaging performance of a 14 × 17-inch Direct Radiography™ System using Se/TFT detector. In: Dobbins III, J.T., Boone, J.M. (eds.) Proc. of SPIE, Medical Imaging 1998: Physics of Medical Imaging, vol. 3336, pp. 14–23. SPIE, Bellingham (1998)
4. Stewart, J.: Calculus: Early Transcendentals, Belmont (2003)
5. Zhao, B., Zhao, W.: Three-dimensional linear system analysis for breast tomosynthesis. Med. Phys. 35(12), 5219–5232 (2008)
6. Barrett, H.H., Myers, K.J.: Foundations of Image Science. Bahaa E.A. Saleh, Hoboken (2004)